Journal of
Materials Chemistry A

Materials for energy and sustainability

Accepted Manuscript

This article can be cited before page numbers have been issued, to do this please use: W. Li, X. Xia and S. Li, *J. Mater. Chem. A*, 2019, DOI: 10.1039/C9TA09227G.

ROYAL SOCIETY OF CHEMISTRY

rsc.li/materials-a

View Article Online
DOI: 10.1039/C9TA09227G

ARTICLE

Large-scale Evaluation of Cascaded Adsorption Heat Pumps Based on Metal/Covalent-Organic Frameworks

Received 00th January 20xx,
Accepted 00th January 20xx

DOI: 10.1039/x0xx00000x

Wei Li, [a,b,c,#] Xiaoxiao Xia [a,b,c,#] and Song Li [a,b,c,*]

Rising demand for living environment and the increasing building energy consumption are creating intense pressure on the develoment of sustainable climate control systems. Cascaded adsorption heat pumps (AHPs) consisting of low-temperature stage (LS) and high-temperature stage (HS) driven by industrial waste heat or renewable energy provide promising solutions. However, their applications are restricted by the low coefficient of performance (COP) mainly due to the unsatisfcatory adsorption perfromance of adsorbents. Here we demonstrated a multiscale computational approach to assess the cooling performance of over three million cascaded AHPs based on novel nanporous metal-organic frameworks (MOFs) and covalent-organic frameworks (COFs). This study demonstrated that MOFs and COFs are favorable for HS and LS of cascaded AHPs, respectively, due to their unique adsorption characteristics. Structure-property analysis revealed that large-pore adsorbents (mostly COFs) exhibiting stepwise adsorption isotherms are more suitable for the COP_C of LS, and small-pore adsorbents (mostly MOFs) exhibiting type I isotherms are beneficial for the COP_C of HS, thus leading to the best performers consisting of COFs in LS and MOFs in HS. Such findings were also validated by experiments. Furthermore, decision tree (DT) analysis hilighted the dominant role of the overall working capacity in determining the cooling performance. We finally demonstrated the succesful implementation of machine learning in speeding up the assessment of a vast number of cascaded AHPs by predicting the COP_C of any adsorbent pairs.

1. Introduction

The rising demand for suitable living environment including heating, cooling and refrigeration has been globally growing,[1] which consumes more than 40% of electricity in the U.S. residential and commercial sectors in 2018.[2] Heat pumps that transfer heat energy in the opposite direction of spontaneous processes are the essential device for these applications. In order to reduce the energy consumption of conventional compression heat pumps powered by electricity, thermally driven adsorption heat pumps (AHPs) that can be driven by waste heat or solar energy are promising alternatives.[3] However, the low thermal efficiency of AHPs because of the low adsorption capacity of adsorbents and poor thermodynamic performance of working pairs[4, 5] greatly limit their application. The basic thermodynamical cycle of AHP systems including adsorption, evaporation, desorption and condensation is frequently employed, whose coefficient of performance for cooling (COP_C) describing the efficiency of adsorption cooling systems is usually low (i.e. $0< COP_C \leq 1$). In contrast, cascaded adsorption heat pumps contain high-temperature stages (HS) and low-temperature stages (LS) by integrating two or more basic thermodynamical cycles in series,[6] which allows for the reuse of heat energy in low-temperature stage (LS) from the high-temperature stage (HS), thus leading to the remarkably enhanced cooling efficiency (i.e. $0 <COP_C \leq 2$).[7]

Various working pairs including silica gel-water[8] and zeolite-water[9, 10] have been investigated for cascaded AHPs. It was revealed that a cascaded AHP based on zeolite and silica gel exhibited a COP_C of 1.35, which is more than two times of that from the basic cycle of AHPs (in most cases, COP_C = 0.5).[8] However, due to the strong interaction between zeolite and working fluids, a high driving temperature is usually required (e.g. 503 K for zeolite[8]). Besides, the low uptake of working fluids is another limiting factor of COP_C. In general, the suitable working pairs of cascaded AHPs should have the following characteristics: (1) the adsorbents of both HS and LS should exhibit the high adsorption capacity of working fluids, i.e. the high overall capacity;(2) the working pairs of HS should exhibit the larger temperature lift than those of LS, suggesting the high desorption temperature of HS than that of LS. Recently, metal-organic frameworks (MOFs)[11] with ultrahigh surface area and pore volume[12] have been recognized as promising adsorbents for AHPs, which could enable record performance.[4,13] A recently reported cascaded AHP system based on two different MOFs gives rise to a record COP_C of 1.63 at low driving temperature of 400 K, implicating the great potential of MOFs for cascaded AHPs.[5]

Given the enormous number of existing MOFs (~10^4), it is impractical to experimentally synthesize all structures and assess the cooling performance of each structure. Besides, the combination of working pairs of HS and LS in cascaded systems could add up to numerous possibilities, from which it is

[a] State Key Laboratory of Coal Combustion, School of Energy and Power Engineering, Huazhong University of Science and Technology, Wuhan 430074, China.
[b] China-EU Institute for Clean and Renewable Energy, Huazhong University of Science and Technology, Wuhan 430074, China.
[c] Nano Interface Centre for Energy, School of Energy and Power Engineering, Huazhong University of Science and Technology, Wuhan 430074, China.
these author contribution equally to this work.
*Corresponding author email: songli@hust.edu.cn.
Electronic Supplementary Information (ESI) available: [details of any supplementary information available should be included here]. See DOI: 10.1039/x0xx00000x

extremely challenging to identify the optimal working pairs for cascaded systems. In previous studies, the adsorption and cooling performance of thousands of MOFs/ethanol and covalent organic frameworks(COFs[14])/ethanol working pairs operated in basic cycle were evaluated by high-throughput computational screening(HTCS) based on integrated grand canonical Monte Carlo (GCMC) simulations and thermodynamical model.[15,16] In comparison with MOFs, COFs preferentially display stepwise adsorption isotherms due to the low affinity towards ethanol. Whereas, a vast number of MOFs exhibited type I adsorption isotherms. Such distinct adsorption behaviours endow MOFs with high temperature lift and COFs with low temperature lift, implicating that combining MOFs for HS with COFs for LS will benefit cascaded AHPs.

In order to increase the diversity of adsorbents (or adsorption isotherms) and improve the chance of discovering the most suitable adsorbent pairs for cascaded systems, both computation-ready experimental (CoRE) MOF and COF databases were taken into account in this work. More than three millions of cascaded AHPs based on the combined MOF and COF adsorbents were evaluated by high-throughput computational screening. Due to the low freezing point, low toxicity, and high heat and mass transfer[4, 17, 18, 19], ethanol was adopted as working fluid in this study. Machine learning was successfully implemented to predict the cooling performance of all working pairs in cascaded AHPs.

2. Computational and experimental methods

2.1. High-throughput computational screening (HTCS)

2.1.1. Structure properties calculations. The computation-ready experimental (CoRE) MOF[20] database comprising 2932 structures and the CoRE COF 2.0[21] database comprising 280 structures in this work. Prior to GCMC simulations, 1264 structures with accessible surface area (ASA) = 0 and two non-MOF structures in the CoRE MOF database were excluded. Meanwhile, one COF exhibiting disordered structure was also removed from CoRE COF database. Therefore, 1666 MOFs and 279 COFs were eventually adopted for HTCS. The largest cavity diameter (LCD), available pore volume (V_a) and accessible surface area (ASA) were computed using a nitrogen probe with a radius of 1.86 Å in Zeo++0.3[22]. The helium void fraction and Henry's constant (K_H) of each structure were calculated by the Widom insertion method[23] in RASPA 1.9.5[24].

2.1.2. COP_C calculation. The COP_C values of LS and HS of all the AHPs under the given working conditions were calculated according to Eq. 1 using the adsorption properties obtained from GCMC simulations.[16] The COP_C of cascaded AHPs is the sum of COP_C of LS and HS.

$$COP_C = \Delta_{vap}H(T_{ev})\rho_{liq}^{wf} m_{sorbent}\Delta W \Big/ \left(\int_I^{III} c_p^{MOFs}(T)dT + \int_I^{II} W_{\max} c_p^{wf}(T)dT + \int_{II}^{III} \frac{W_{\max}+W_{\min}}{2} c_p^{wf}(T)dT - \frac{1}{M_w}\int_{W_{\min}}^{W_{\max}} \Delta_{ads}H(W)dW\right) \quad (1)$$

$\Delta_{vap}H$ is the evaporation enthalpy of ethanol at evaporation temperature T_{ev}, ρ_{liq}^{wf} is the density of liquid ethanol adsorbates, $m_{sorbent}$ is the mass of the MOF adsorbents, ΔW is the working capacity between the $W_{\max}$ (I to II, Fig. 1) at the adsorption stage and the $W_{\min}$ (III to IV, Fig. 1) at the desorption stage. c_p^{MOFs} and c_p^{wf} are the heat capacity of the adsorbents and working fluids, respectively. M_w is the molar mass of the working fluids. $\Delta_{ads}H$ is the enthalpy of adsorption.

2.1.3. GCMC simulation. A two-stage thermodynamical cycle (Fig. 1) of cascaded AHP under the predefined working condition (Table 1) was used for GCMC simulation. According to the isosteric diagram of cascaded AHPs in Fig. 1, there are two stages including low-temperature stage (LS) and high-temperature stage (HS) in the cycle. The detailed working conditions provided in Table 1 were taken from previous study[5]. The evaporation temperature (T_{ev}) represent the temperature of evaporator and the target cooling temperature that AHPs can achieve. The condensation temperature (T_{con}) represent the temperature of the condenser, which is usually identical to ambient temperature and adsorption temperature(T_{ads}). The adsorption (T_{ads}) and desorption temperature (T_{des}) indicate the adsorption bed temperature in the beginning of adsorption and desorption, respectively. The evaporation pressure (P_{ev}) and condensation pressure (P_{con}) represent the saturation pressure of working fluid at T_{ev} and T_{con}, respectively. The difference between condensation and evaporation temperatures is temperature lift. The minimal desorption or maximal preheating temperature (T_2) in each stage was obtained from Trouton's rule[25].

2.1.4.

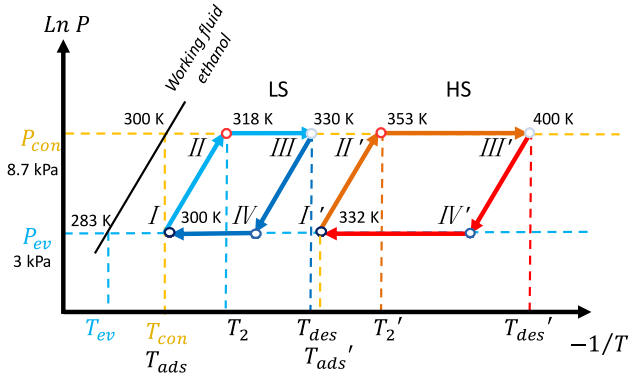

Fig. 1. Isosteric diagram of cascaded adsorption heat pumps consisting of low-temperature stage (LS, I to IV) and high-temperature stage (HS, I' to IV'). The evaporation temperature (T_{ev} = 283 K), condensation temperature (T_{con} = 300 K), evaporation pressure (P_{ev}= 3 kPa) and condensation pressure (P_{con}= 8.7 kPa) were used. The adsorption temperature (T_{ads}) desorption temperature (T_{des}) of LS and HS were specified in Table 1.

Table 1. The working conditions of each stage in cascaded AHPs.

Stage	Step	Temperature (K)	Pressure (kPa)
LS	I	T_{ads} = 300	P_{ev} = 3
	II	T_2 = 318	P_{con} = 8.7
	III	T_{des} = 330	P_{con} = 8.7
HS	I'	T_{ads} = 332	P_{ev} =3

II'	T_2 = 353	P_{con} = 8.7
III'	T_{des} = 400	P_{con} = 8.7

GCMC simulations were implemented for MOFs and COFs to obtain their ethanol adsorption isotherms and enthalpy of adsorption at defined working conditions. LJ parameters of all the MOFs and COFs were taken from the UFF force field[26]. TraPPE force field[27] was used for ethanol in Table S1, the reliability of UFF and TraPPE force field in describing the adsorption properties has been demonstrated in previous studies[28, 29]. Four types of Monte Carlo moves including insertion, deletion, rotation and translation were implemented with equal probability. In the initial round, a total of 4×10^4 cycles were performed for MOFs and COFs to estimate the ethanol uptakes and heat of desorption, including 2×10^4 cycles of equilibration runs and 2×10^4 cycles of production runs. Under LS conditions, there are 119 MOFs and 1 COF exhibiting the working capacity (ΔW) below zero, which is due to the remarkable fluctuation in the uptakes of structures at adsorption and desorption process, and insufficient equilibration. Besides, 121 MOFs and 7 COFs with unreasonable heat of desorption ($\Delta_{ads}H$ = inf) due to the extremely low uptakes were also excluded from the following rounds. Similarly, under HS condition, 3 MOFs exhibiting ΔW < 0, and 70 MOFs and 6 COFs with unreasonable heat of desorption ($\Delta_{ads}H$ = inf) were excluded. Therefore, eventually approximately three million (i.e. 3,166,602) two-stage AHPs by combining the adsorbents of LS and HS were evaluated for the subsequent screening. After obtaining the COP_C from the initial round, the adsorbent pairs with COP_C above 1.6 were selected for the second round, in which 4×10^5 Monte Carlo cycles were performed. In the final round, any adsorbent pair with COP_C above 1.6 were chosen for GCMC simulation, where more than 1×10^5 cycles were implemented until achieving complete equilibration. Similar approach has been reported in previous work[16, 30], which can be completed within reasonable computational cost. It should be noted that such a strategy may exclude some potential candidates from the initial round of screening. However, this approach was still adopted in this work to reach a compromise between the computational cost and the number of selected high-performing candidates from screening. The high possibility of including a large amount of potential candidates in the final round has been validated in the evolutionary trends of Fig.S7-9, from which all remained structures in the final round do exhibit the favorable structure properties as well as high COP_C. Eventually, 3,404 cascaded AHPs with COP_C >1.6 composed of 10 MOFs and 36 COFs in the LS, and 66 MOFs and 8 COFs in HS were identified from the final round as shown in Table S2, S3, S4 and S5.

View Article Online DOI: 10.1039/C9TA09275F

2.2. Experimental validation

In order to verify the trend observed in HTCS, two widely investigated MOFs(Cu-BTC[31], MIL-101(Cr)[32]) and COFs (COF-1[33] and COF-5[34]),were synthesized. Their ethanol adsorption isotherms were measured at 288 K and 298 K (the detailed information can be found in SI), from which the COP_C of 16 cascaded AHPs can be calculated according to the thermodynamical cycle of cascaded AHPs as reported in previous work.[16] The only modification is that the heat capacity of working fluids was taken into account in this work.

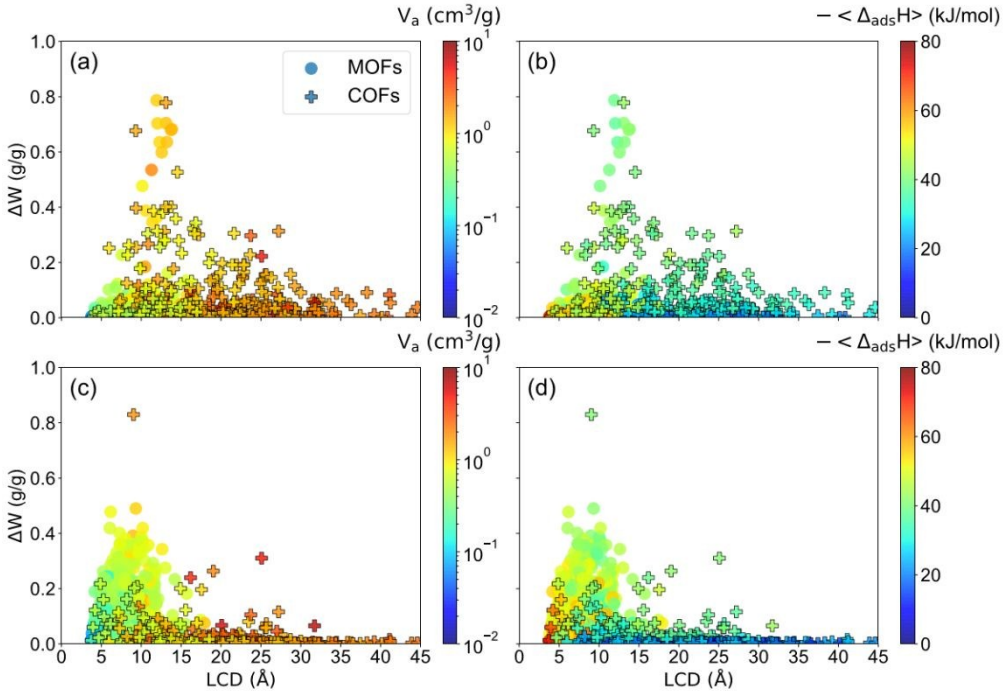

Fig. 2 (a) Predicted ΔW values of 1426 MOFs and 271 COFs in LS as a function of LCD, (a) colored by V_a and (b) colored by $-<\Delta_{ads}H>$. 1593 MOFs and 273 COFs in HS as a function of LCD , (c) colored by V_a and (d) colored by $-<\Delta_{ads}H>$. ΔW was obtained from the difference in the ethanol uptake between the uptakes at T_2 = 318 K and T_{des} = 330 K (LS), and T_2'= 332 K and T_{des}' = 400 K (HS) at condensation pressure (p_{con} = 8.7 kPa).

2.3. Data Mining and Machine Learning

3,166,602 cascaded AHPs were used for decision tree (DT), the maximum depth layer for decision tree is three, in which ΔW, $-<\Delta_{ads}H>$, LCD, ASA and V_a were taken into consideration. In order to quickly estimate the cooling performance of adsorbent pairs in cascaded AHP systems, different machine learning algorithms

including multiple linear regression (MLR), decision tree (DT), gradient boosting machine (GBM) and random forest (RF) were tested. 20% of samples were randomly chosen for training, and the rest 80% were used as test set. Six descriptors including LCD, ASA, void fraction (VF), V_a, K_H and MOF density (ρ) were used for varying machine learning algorithms. The accuracy of each model was evaluated by R^2.

3 Results and discussion

3.1. COP_C of LS and HS of cascaded AHPs

As mentioned before, the overall capacity is critical for the cooling performance of AHPs. The adsorption performance of MOFs and COFs in LS and HS under given working conditions obtained from the first-round screening were analysed (Fig. 2). The correlation between structure properties (LCD, V_a) and adsorption performances (ΔW, $<\Delta_{ads}H>$) of LS and HS were presented. It was found that at LS, most of COFs exhibited the higher ΔW than MOFs (Fig. 2a and 2b), which is reversed at HS (Fig.2c and 2d). Such phenomena suggested that the use of COFs at LS and MOFs at HS may be an optimal combination for cascaded AHPs. Furthermore, at LS, both MOFs and COFs with high working capacity (ΔW > 0.2 g/g) exhibited the pore size of 10 – 15 Å and the high pore volume (V_a ~ 2 cm^3/g). Nevertheless, at HS, the structures with ΔW > 0.2 g/g displayed the pore size of 5 – 12.5 Å with smaller pore volume (V_a ~ 1 cm^3/g). However, the average enthalpy of adsorption ($-<\Delta_{ads}H>$) of those structures are located at approximately 40 kJ/mol. The pore size of most CoRE MOFs are lower than 15 Å, whereas COFs exhibited the wider pore size range, indicating the different preference of structure properties of adsorbents at LS and HS that will be discussed later.

The COP_C of LS and HS (Fig. 3) suggested that both MOFs and COFs exhibited the higher COP_C at LS than HS, which is mostly due to the high working capacity at LS and high sensible heat required at HS. At LS, MOFs and COFs with COP_C > 0.8 displayed the pore sizes of 7.5 – 17.5 Å and 7.5 – 37.5 Å, respectively. At HS, MOFs and COFs with COP_C > 0.8 have relatively small pore sizes of 7.5 -12.5 Å and 7.5-10 Å, respectively, consistent with the tendency in working capacity of Fig. 2. These results illustrated the importance of choosing suitable adsorbent pairs for LS and HS to optimize the COP_C of cascaded AHP systems.

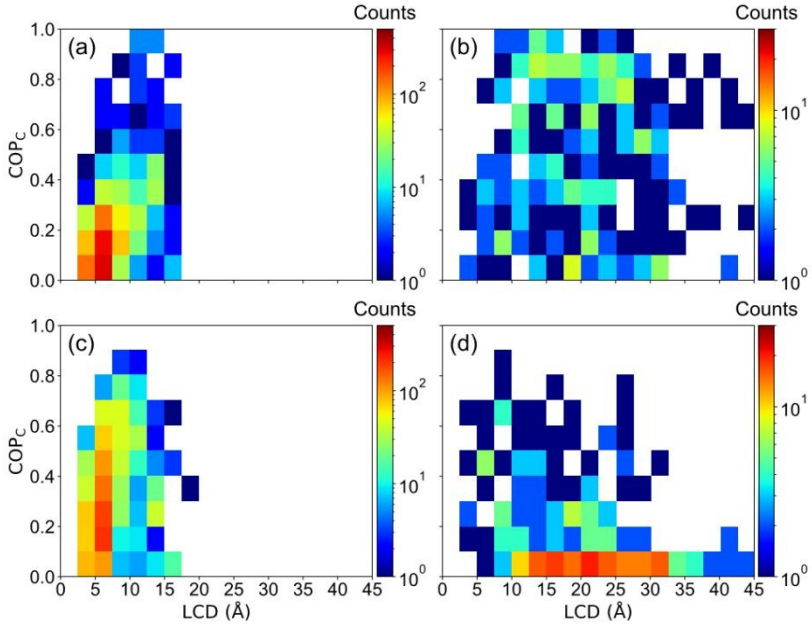

Fig. 3. The number distributions of (a,c) MOFs and (b,d) COFs with varying COP_C and LCD in (a,b) LS and(c,d) HS.

3.2. The overall COP_C of cascaded AHPs

The overall COP_C of cascaded AHP systems is the sum of COP_C of LS and HS. Among the 3,166,602 cascaded AHPs, there are 1688 AHPs based on identical adsorbents for LS and HS, and approximately three million AHPs composed of different adsorbents for LS and HS. The AHPs can be generally classified into two possible combinations: 1) identical adsorbents for LS and HS (A_{ad}+A_{ad}), and 2)different adsorbents for LS and HS (A_{ad}+B_{ad}). To find out the more promising combination, the overall COP_C of the two combinations were analysed in Fig. 4a, from which it can be found that the overall COP_C of cascaded AHPs based on identical adsorbents for LS and HS is lower than 1.6. In contrast, the cascaded AHP systems consisting of two different adsorbents for LS and HS can achieve COP_C > 1.6, which can be probably ascribed to the high diversity of such a combination resulting from the large number of AHPs of this combination. More specifically, from the perspective of material type, the cascaded AHPs can be divided into four types: 1) MOFs for LS and HS (MOF_{LS} + MOF_{HS}), 2) MOFs for LS and COFs for HS (MOF_{LS} + COF_{HS}),3) COFs for LS and MOFs for HS (labelled as COF_{LS} + MOF_{HS}), and 4) COF for LS and HS (COF_{LS} + COF_{HS}). The overall COP_C of the four types are shown in Fig. 4b. Although there is no evident discrepancy in maximum COP_C of each type, the average COP_C of cascaded AHPs using COFs for LS and MOFs for HS (COF_{LS} + MOF_{HS}) is significantly higher than the other three types of combinations, followed by COF_{LS} + COF_{HS} (type 4), MOF_{LS} + MOF_{HS} (type 1) and MOF_{LS} + COF_{HS} (type 2). Such a tendency suggested that COFs are suitable adsorbents for LS and MOFs are favourable for HS, leading to the overall high cooling performance of cascaded AHP systems.

View Article Online
DOI: 10.1039/C9TA09227G

ARTICLE

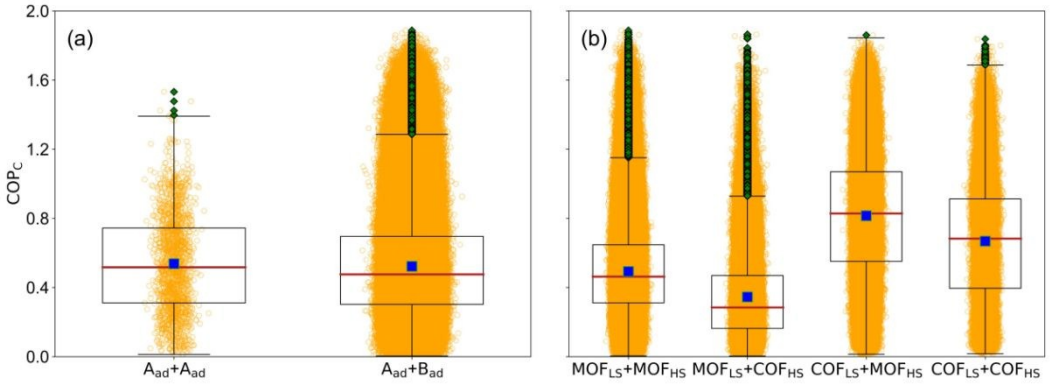

Fig. 4. The COP_C distribution of cascaded AHPs using (a) identical adsorbents at LS and HS ($A_{ad}+A_{ad}$) and different adsorbents for LS and HS ($A_{ad}+B_{ad}$); (b) the COP_C distribution of cascaded AHPs based on the four types of adsorbent combinations for LS and HS.

Since the combination of COF_{LS} + MOF_{HS} provides a large number of best performers for cascaded AHP_S, in the following analysis, we mainly focused on their structure-property relationship. The correlation between overall COP_C of cascaded AHPs and the pore sizes of their adsorbents of LS (LCD_{LS}) and HS (LCD_{HS}) in Fig. 5a shown that the AHPs with the highest COP_C displayed the LCD_{LS}/LCD_{HS} = 1.5 and LCD_{LS} of approximately 15 Å, implicating that adsorbents of LS should possess the larger pore size than that of HS, consistent with previous finding.[5] However, further increase in the pore size of adsorbents at LS will not enhance the cooling performance due to the reduced overall working capacity (Fig.2). Most of AHPs are based on the combination of COF_{LS} + MOF_{HS} (Fig.5b), which is more evident in Fig S2. The AHPs of other types did not have so many adsorbent pairs exhibiting preferential pore sizes range (Figure S2 and Fig. S3a-c). Similar tendencies were observed in pore volume ratio (Fig.5c-d) and surface area (Fig.S4). It was found that the favourable pore volume ratio for the overall COP_C is V_{LS}/V_{HS} = 2 with V_{LS} = 2 cm^3/g (Fig. 5c) and ASA_{LS}/ASA_{HS} = 2 with ASA_{LS} = 3000 m^2/g, consistent with the pore size ratio. Most of AHPs with COF_{LS} + MOF_{HS} are located in this range (Fig.5d and Fig.S4b). In general, the adsorbents of LS with the slightly larger LCD, V_a and ASA than those of HS are favourable for COP_C. Such a tendency may be also related with the different adsorbent-adsorbate interaction strength or the shape of adsorption isotherms between LS and HS. It has been known that the adsorbents of HS should be able to sustain the high desorption temperature, implicating strong adsorbent-adsorbate interaction; whereas relatively low desorption temperature for the adsorbents of LS is required, indicating the weak adsorbent-adsorbate interaction.

View Article Online
DOI: 10.1039/C9TA09227G

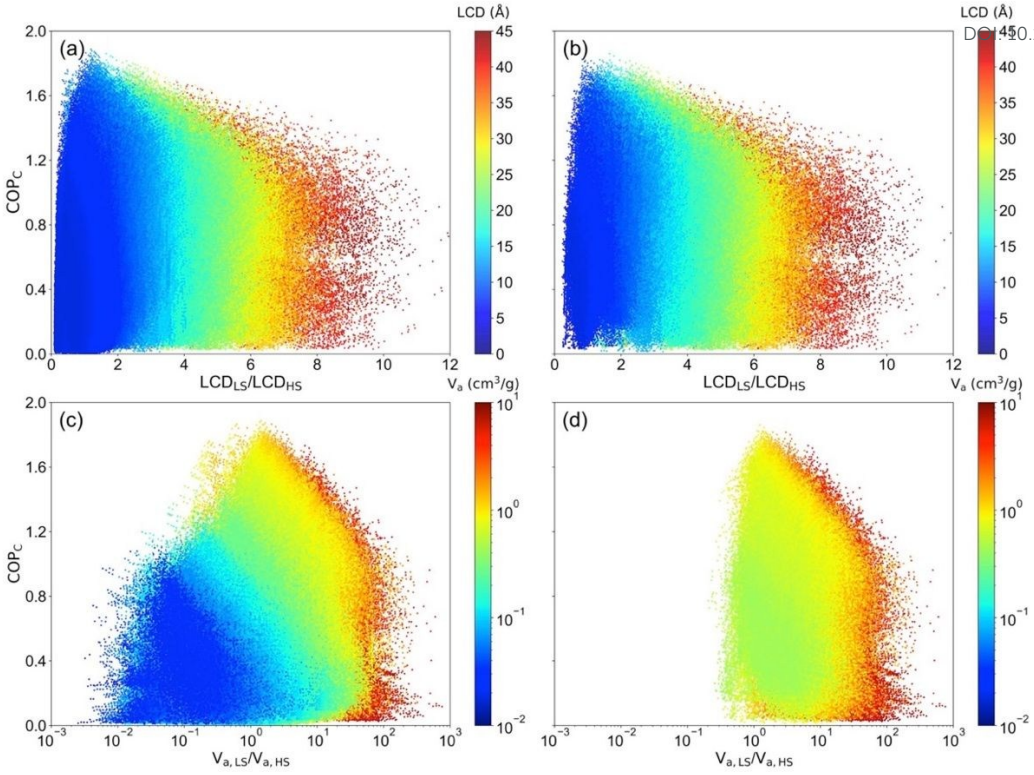

Fig. 5. The COP_C distribution of cascaded AHPs with the various structure properties between low stage and high stage. (a) The COP change with the LCD_{LS}/LCD_{HS} of 3,166,602 cascaded AHPs. (b) The COP change with the LCD_{LS}/LCD_{HS} of 431,703 COF_{LS} + MOF_{HS} cascaded AHPs. (c) The COP change with the $V_{a,\ LS}/V_{a,\ HS}$ of 3,166,602 cascaded AHPs. (d) The COP change with the $V_{a,\ LS}/V_{a,\ HS}$ of 431,703 COF_{LS} + MOF_{HS} cascaded AHPs.

To evaluate the adsorbent-adsorbate interaction of LS and HS, Henry's constant (K_H) that describes the affinity towards adsorbate at ultralow pressure were calculated (Fig.6). Fig. 6a demonstrated that the high-performing cascaded AHPs exhibited $K_{H,LS}/K_{H,HS}$ = 0.1 with $K_{H,LS}$ = 10^{-4} mol/kg·Pa, suggesting that the adsorbents of LS exhibiting weak interaction and the adsorbents of HS exhibiting strong interaction towards working fluids are preferential for COP_C. In other words, the adsorbents in LS with stepwise adsorption isotherms and the adsorbents of HS with type I adsorption isotherm will benefit the cooling performance of cascaded AHPs. The steps location (α) of adsorption isotherms of MOFs and COFs at LS and HS conditions (Fig.6c, d, e and f) validated that adsorbents with the high steps at LS (MOFs with 0.1 < α < 0.2 and COFs with 0.2 < α < 0.6) and adsorbents with low steps at HS (MOFs with 0 < α < 0.1 and COFs with 0 < α < 0.2) are favourable for COP_C . Similarly, COFs at LS and MOFs at HS are the best adsorbent pairs for cascaded AHPs, which exhibits preferential $K_{H,LS}/K_{H,HS}$ (Fig.6b) and adsorption isotherms. Such a tendency agrees with previous study on cascaded AHPs using MOF-water working pairs, in which the use of hydrophobic MOF of LS and hydrophilic MOF of HS can benefit the cooling efficiency.[5]

View Article Online
DOI: 10.1039/C9TA09227G

ARTICLE

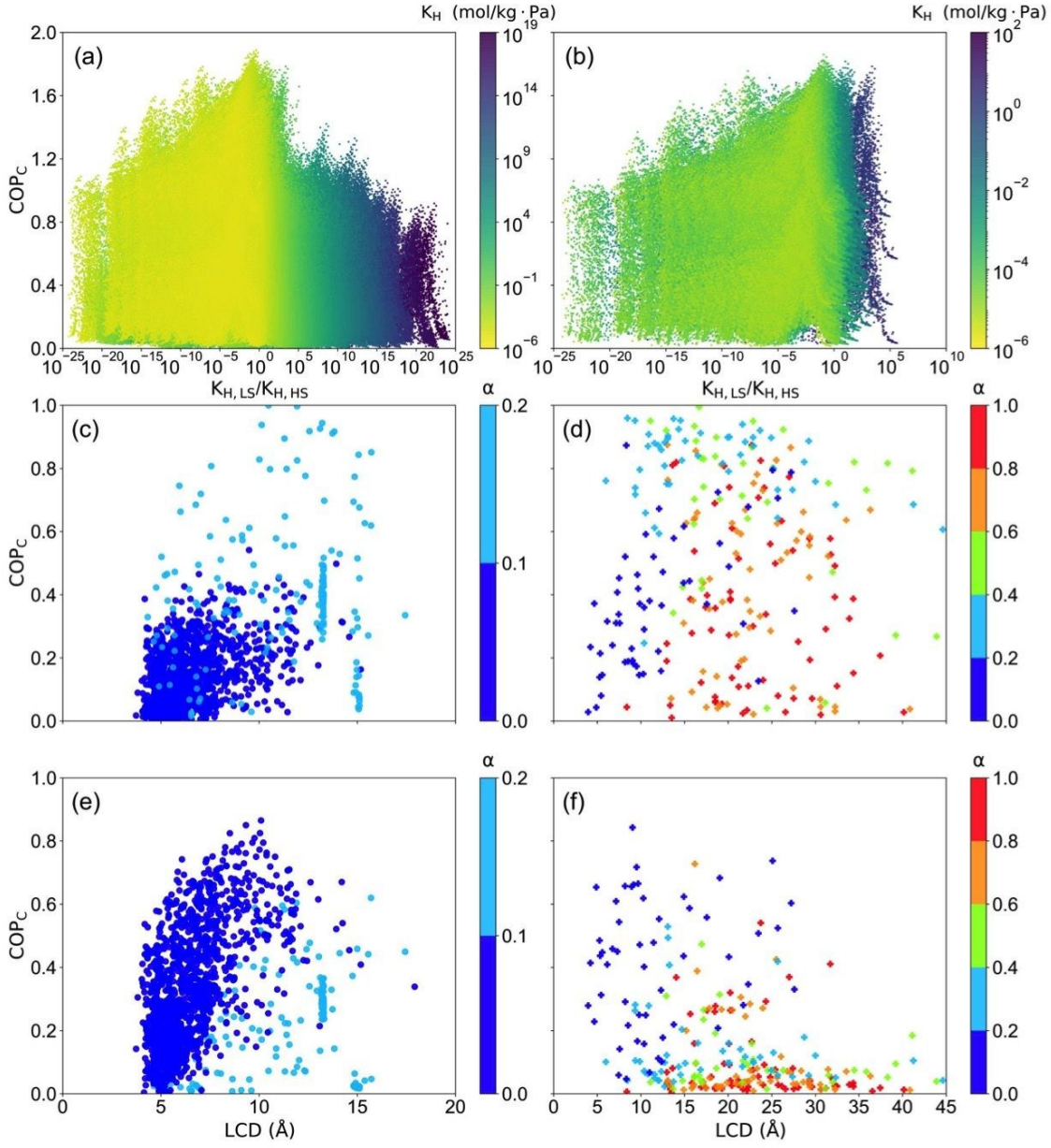

Fig. 6. (a) The COP_C of total 3 166 602 cascaded AHPs as a function of $K_{H,LS}/K_{H,HS}$; (b) The COP_C of 431 703 cascaded AHPs consisting of COFs for LS and MOFs for HS(COF_{LS}+ MOF_{HS}) as a function of $K_{H,LS}/K_{H,HS}$. The relationship between COP_C and LCD of (c) MOFs in LS, (d) COFs in LS, (e) MOFs in HS, (f) COFs in HS, colored by alpha point(α).

From the three-round computational screening, 3,404 cascaded AHPs with COP_C > 1.6 consisting of 10 MOFs (Table S2)and 36 COFs (Table S3) for LS, and 66 MOFs (Table S4) and 8 COFs (Table S5) for HS were identified, validating the preference of COFs for LS and MOFs for HS. On the other hand, with the progress of screening, the evolution of structure and adsorption properties of adsorbents in cascaded AHP systems can be obtained (Fig. S7). According to the evolution of pore size (LCD), pore volumes (V_a), working capacities (ΔW) and load average enthalpy of adsorption ($-<\Delta_{ads}H>$) of MOFs and COFs of LS and HS from the first to the final round of screening(Fig. S8 and Fig. S9), it was revealed that the screening evolved the MOFs of LS with the slightly larger pore size (10 < LCD < 15 Å), pore volume (V_a > 1 cm^3/g) and moderate average enthalpy of adsorption (40 < $-<\Delta_{ads}H>$ ≤ 60 kJ/mol). However, MOFs of HS with the smaller pore size (5 < LCD < 10 Å), pore volume (0.5 < V_a < 0.75 cm^3/g) and moderate average enthalpy of adsorption (40 < $-<\Delta_{ads}H>$ ≤ 60 kJ/mol) are preferred. Similar trends were observed for COFs of LS and HS, suggesting that large-pore adsorbents are favourable for

LS and small-pore adsorbents are more suitable for HS. Regardless of adsorbents of LS and HS, moderate average enthalpy of adsorption ($40 < -\langle\Delta_{ads}H\rangle \leq 60$ kJ/mol) and high ΔW are beneficial for the cooling efficiency.

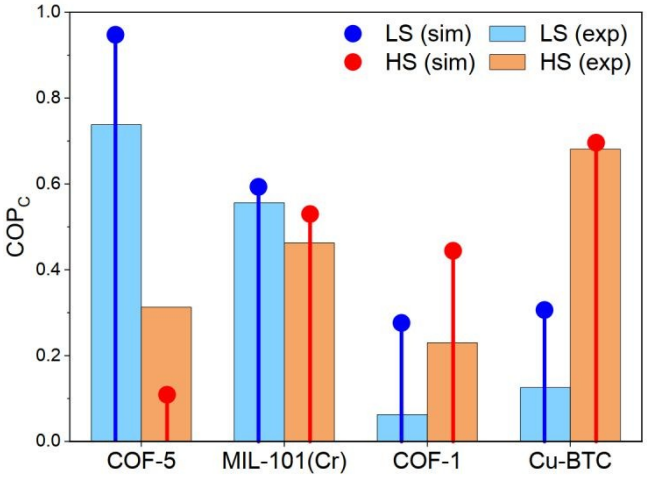

Fig. 7. Comparison of COP_C of LS and HS obtained from prediction and experiments.

In order to verify the trend above, two most widely investigated MOFs and two COFs with varying pore sizes were synthesized and tested. According to the measured adsorption isotherms of small-pore COF-1 (~1.06 nm) and Cu-BTC (~1.1 nm), and large-pore COF-5 (~2.58 nm) and MIL-101(Cr) (~2.58 nm), the COP_C of these structures for LS and HS of cascaded systems were obtained(Fig. 7), which shown that the large-pore COF performed better than MOF in LS, and small-pore MOF perform better than COF in HS. Such results suggested the reliability of the reported trend in this work regardless of the deviation in ethanol adsorption isotherms of COFs observed between experiments and simulations (Fig. S15) due to the poor crystallinity of COFs [35-37].

3.3. Data Mining and Machine Learning

To further clarify the role of the correlation between various structure and adsorption characteristics of adsorbents with cooling performance of cascaded AHPs, decision tree (DT) model was applied to elucidate the route to identify the high-performance cascaded AHP systems. DT model analysis of 3,166,602 cascaded AHP systems in Fig. 8 shown that the working capacity (ΔW) plays a dominant role in COP_C. There are generally seven routes from the DT analysis. It can be found that the working capacity of LS (ΔW_{LS}) dominates the overall COP_C of cascaded AHPs, in which $COP_C > 1.6$ when $\Delta W_{LS} > 0.18$ g/g. In the secondary layer, the working capacity of HS (ΔW_{HS}) dominates, and most of the high-performing AHPs ($COP_C > 1.6$) possess the beneficial combination of $COF_{LS} + MOF_{HS}$.

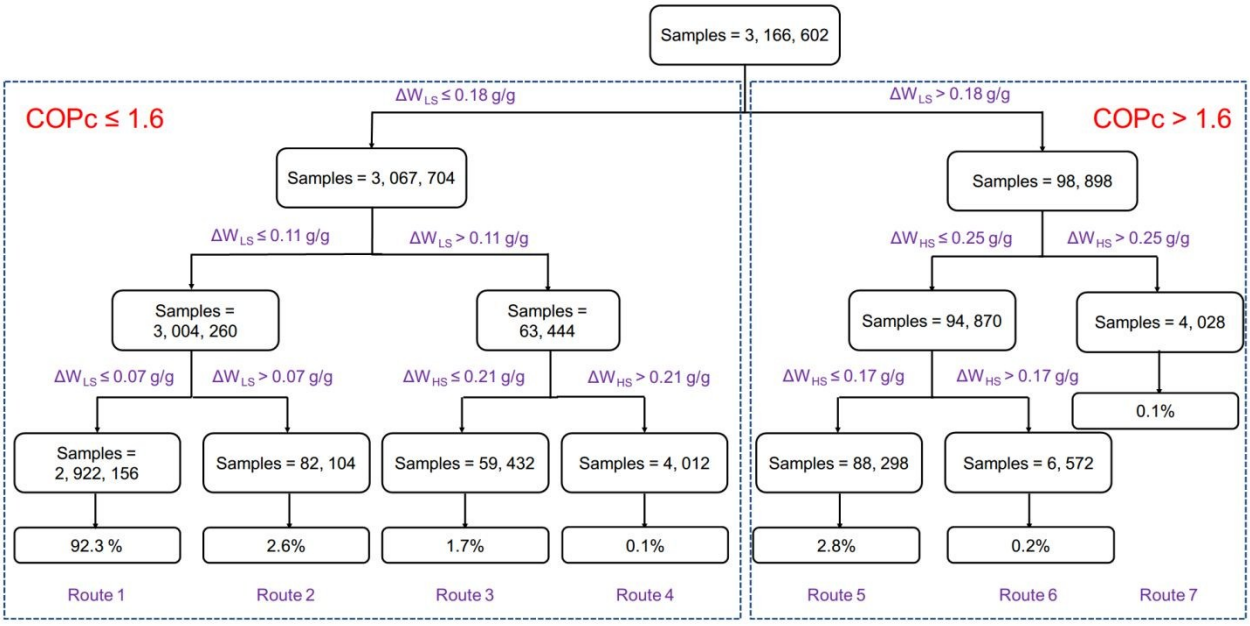

Fig. 8. Decision tree of 3,166,602 cascaded AHPs.

Given the critical roles of ΔW_{LS} and ΔW_{HS} in determining the cooling performance of cascaded adsorption heat pumps, the correlation between the overall COP_C and the overall working capacity was elucidated (Fig.9a). The higher the sum of working capacity of LS and HS ($\Delta W_{LS} + \Delta W_{HS}$), the higher cooling performance, which is consistent with the tendency in single-stage AHPs. When $\Delta W_{LS} + \Delta W_{HS} > 0.4$ g/g, there is no remarkable enhancement in the overall COP_C. Besides, the average enthalpy of adsorption $-\langle\Delta_{ads}H\rangle$ of each stage is another important factor affecting the COP_C. The high $-\langle\Delta_{ads}H\rangle$ (60 kJ/mol< $-\langle\Delta_{ads}H\rangle$ <100 kJ/mol) definitely resulted in the reduced overall COP_C. Whereas the low $-\langle\Delta_{ads}H\rangle$ (0 kJ/mol< $-\langle\Delta_{ads}H\rangle$ <40 kJ/mol) may give rise to high COP_C, but the working capacity of such cascaded AHPs are too low. Only moderate $-\langle\Delta_{ads}H\rangle$ is favorable for both COP_C and the overall working capacity. It was also revealed that both $-\langle\Delta_{ads}H\rangle_{LS}$ and $-\langle\Delta_{ads}H\rangle_{HS}$ should be at moderate range (~40 kJ/mol) to achieve the high overall cooling performance

View Article Online
DOI: 10.1039/C9TA09227G

(Fig.9b). Similarly, most of the AHPs with the combination of COF_{LS} + MOF_{HS} possess the suitable $-<\Delta_{ads}H>_{LS}$ and $-<\Delta_{ads}H>_{HS}$ (Fig. S20).

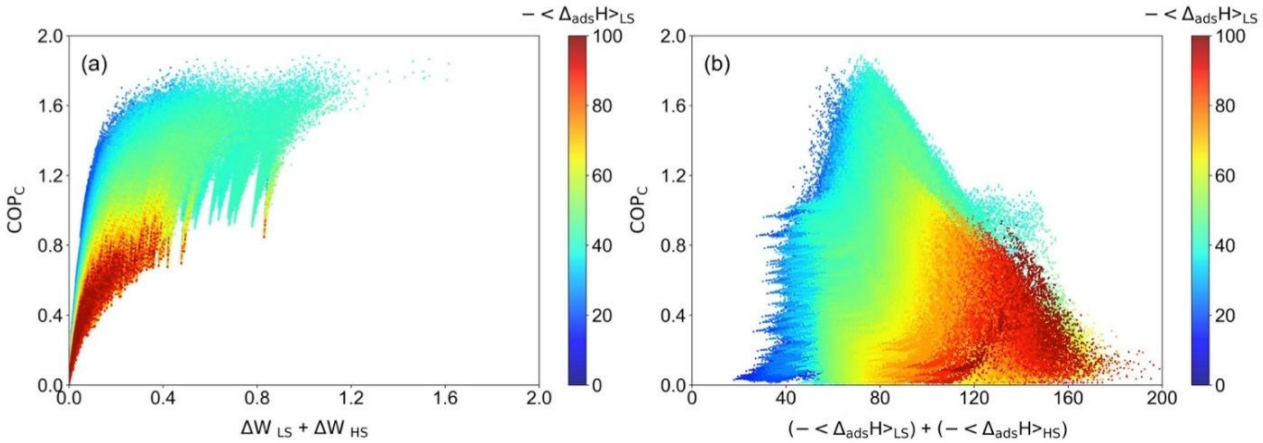

Fig. 9. (a) The relationship between $\Delta W_{LS} + \Delta W_{HS}$ and COP_C, colored by $-<\Delta_{ads}H>_{LS}$. (b) The relationship between $(-<\Delta_{ads}H>_{LS}) + (-<\Delta_{ads}H>_{HS})$ and COP_C, colored by $-<\Delta_{ads}H>_{LS}$.

Given the large diversity in the combinations of adsorbents in LS and HS, predicting the cooling performance of cascaded AHP systems based on GCMC simulations can be extremely time-consuming and expensive. Therefore, machine learning (ML) was implemented to accelerate the process of identifying high-performing cascaded AHPs by the quantitative structure-property correlations. In this work, various machine learning algorithms including multiple linear regression (MLR), decision tree (DT), gradient boosting machine (GBM) and random forest (RF) were used for predicting the COP_C by using the data from high-throughput computational screening. Six descriptors including largest cavity diameter (LCD), accessible surface area (ASA), void fraction (VF), available pore volume (V_a), Henry's constant (K_H) and density of structures (ρ) were used for training of the dataset. According to Fig. S22, the 20% samples for training are sufficient to give rise to the satisfactory prediction accuracy. Thus, 20% samples was used for training and the 80% was used for test. Among various ML algorithms, RF model shown the highest prediction accuracy (R^2 = 0.95), followed by GBM (R^2=0.94), DT (R^2=0.91) and MLR (R^2=0.13) (Fig. 10), suggesting the success of RF model in COP_C prediction of cascaded AHPs. The average computation time for each cascaded AHP by GCMC simulation 4.09 seconds, which is approximately three orders of magnitude of that by machine learning (0.003 second), indicating significantly accelerated screening process by machine learning. The relative importance of varying descriptors of adsorbents in LS and HS by RF model in Fig. 10e-f demonstrated that V_a (24.99%) contributed most to the COP_C of LS, which may be due to the dominant role of pore volume in the maximum uptake of adsorbents of LS. In HS, K_H(23.58%) contributed most to the COP_C, suggesting the importance of the affinity between adsorbents and working fluids, or the shape of adsorption isotherm in determining cooling performance of HS in cascaded AHPs .

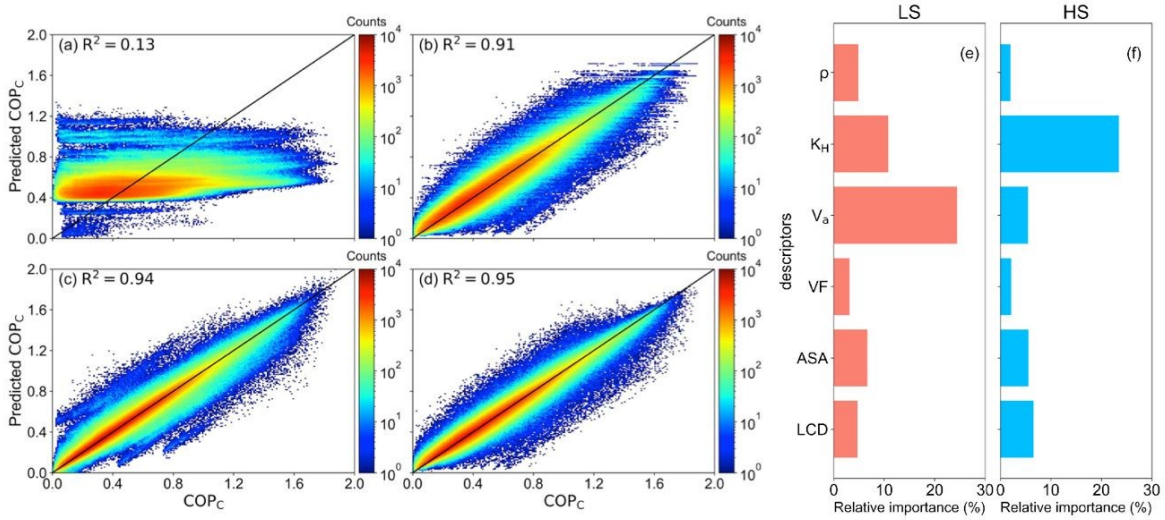

Fig. 10. COP_C predicted by varying machine learning models (a) MLR, (b) DT, (c) GBM, (d) RF colored by the number density of cascaded AHPs. For each model, 20% samples were randomly chosen as training dataset and the rest 80% were used as test dataset. The relative importance of six descriptors including LCD, ASA, VF, V_a, K_H and MOF density (ρ) from the RF model in COP_C of (e) LS and (f) HS.

View Article Online
DOI: 10.1039/C9TA09227G

4. Conclusions

In this work, we evaluated the cooling performance of over three million cascaded AHPs based on MOF and COF adsorbents by high-throughput computational screening. It was revealed that COFs and MOFs are preferential adsorbents for LS and HS, respectively. Structure-property relationship analysis demonstrated the high-performing adsorbents for cascaded AHPs should exhibit the following characteristics: 1) the overall high working capacity of LS and HS;2) the moderate average enthalpy of adsorption for adsorbents in both LS and HS; 3)the big pore sizes of adsorbents in LS than that in HS ;4) the lower Henry's constant of adsorbents in LS than that of HS, i.e. the preferential stepwise adsorption isotherms of adsorbents for LS and type I isotherms of adsorbents for HS. The dominant role of working capacity of LS was illustrated by DT analysis and the correlation between the overall working capacity, enthalpy of adsorption and the COP_C were further verified. Machine learning was successfully implemented to predict the overall COP_C of cascaded AHPs of all adsorbent pairs, indicating the accelerated development of high-efficient cascaded AHPs by quick discovery of potential adsorbents. This study highlights the potential use of novel adsorbent pairs, i.e. MOFs and COFs in cascaded AHPs for the first time. Our findings may provide useful insights into efficiently exploring high-performing adsorbents for improved cooling performance of cascaded AHPs.

Conflicts of interest

There are no conflicts of interests to declare.

Acknowledgements

This work was supported by the National Natural Science Foundation of China (NSFC) under Project No. 51606081 and Hubei Provincial Nature Science Foundation(No. 2019CFB456). This work was also supported by THE double first-class research funding of China-EU Institute for Clean and Renewable Energy (No. ICARE-RP-2018-HYDRO-001) and the Graduates' Innovation Fund of Huazhong University of Science and Technology (No. 2019YGSCXCY026). We thank the support from Analytical & Testing Center of Huazhong University of Science and Technology, and the National Supercomputer Center of Shenzhen.

Notes and references

1. A. Reese, *Science*, 2018, **359**, 1084-1084.
2. *Annual energy outlook* U.S. Energy Information Agency, 2019.
3. N. Zhou, N. Khanna, W. Feng, J. Ke and M. Levine, *Nature Energy*, 2018, **3**, 978-984.
4. M. F. de Lange, K. J. F. M. Verouden, T. J. H. Vlugt, J. Gascon and F. Kapteijn, *Chemical Reviews*, 2015, **115**, 12205-12250.
5. A. J. Rieth, A. M. Wright, S. Rao, H. Kim, A. D. LaPotin, E. N. Wang and M. Dincă, *Journal of the American Chemical Society*, 2018, **140**, 17591-17596.
6. F. Meunier, *Journal of Heat Recovery Systems*, 1986, **6**, 491-498.
7. F. Meunier, *Journal of Heat Recovery Systems*, 1985, **5**, 133-141.
8. Y. Liu and K. C. Leong, *International Journal of Refrigeration*, 2006, **29**, 250-259.
9. N. Douss and F. Meunier, *Chemical Engineering Science*, 1989, **44**, 225-235.
10. B. Dawoud, *Renewable Energy*, 2007, **32**, 947-964.
11. H. Furukawa, K. E. Cordova, M. O'Keeffe and O. M. Yaghi, *Science*, 2013, **341**, 1230444.
12. R. B. Getman, Y. S. Bae, C. E. Wilmer and R. Q. Snurr, *Chemical Reviews*, 2012, **112**, 703-723.
13. S. Wang, J. S. Lee, M. Wahiduzzaman, J. Park, M. Muschi, C. Martineau-Corcos, A. Tissot, K. H. Cho, J. Marrot, W. Shepard, G. Maurin, J.-S. Chang and C. Serre, *Nature Energy*, 2018, **3**, 985-993.
14. S. Y. Ding and W. Wang, *Chemical Society Reviews*, 2013, **42**, 548-568.
15. M. Erdos, M. F. de Lange, F. Kapteijn, O. A. Moultos and T. J. H. Vlugt, *Acs Applied Materials & Interfaces*, 2018, **10**, 27074-27087.
16. W. Li, X. Xia, M. Cao and S. Li, *Journal of Materials Chemistry A*, 2019, **7**, 7470-7479.
17. M. F. de Lange, B. L. van Velzen, C. P. Ottevanger, K. J. Verouden, L. C. Lin, T. J. Vlugt, J. Gascon and F. Kapteijn, *Langmuir*, 2015, **31**, 12783-12796.
18. H. Chen, Z. Chen, L. Zhang, P. Li, J. Liu, L. R. Redfern, S. Moribe, Q. Cui, R. Q. Snurr and O. K. Farha, *Chemistry of Materials*, 2019, **31**, 2702-2706.
19. R. Wang, L. Wang and J. Wu, *Adsorption refrigeration technology: theory and application*, John Wiley & Sons, Singapore, 2014.
20. D. Nazarian, J. S. Camp and D. S. Sholl, *Chemistry of Materials*, 2016, **28**, 785-793.
21. M. Tong, Y. Lan, Z. Qin and C. Zhong, *The Journal of Physical Chemistry C*, 2018, **122**, 13009-13016.
22. T. F. Willems, C. H. Rycroft, M. Kazi, J. C. Meza and M. Haranczyk, *Microporous and Mesoporous Materials*, 2012, **149**, 134-141.
23. B. Widom, *The Journal of Chemical Physics*, 1963, **39**, 2808-2812.
24. D. Dubbeldam, S. Calero, D. E. Ellis and R. Q. Snurr, *Molecular Simulation*, 2016, **42**, 81-101.
25. Y. I. Aristov, *Journal of Chemical Engineering of Japan*, 2007, **advpub**, 0710050048-0710050048.
26. A. K. Rappe, C. J. Casewit, K. S. Colwell, W. A. Goddard, III and W. M. Skiff, *J. Am. Chem. Soc.*, 1992, **114**, 10024-10035.

View Article Online
DOI: 10.1039/C9TA09227G

27. B. Chen, J. J. Potoff and J. I. Siepmann, *Journal of Physical Chemistry B*, 2001, **105**, 3093-3104.
28. A. Nalaparaju, X. S. Zhao and J. W. Jiang, *The Journal of Physical Chemistry C*, 2010, **114**, 11542-11550.
29. R. Bueno-Perez, P. J. Merkling, P. Gómez-Álvarez and S. Calero, *Chemistry – A European Journal*, 2017, **23**, 874-885.
30. C. E. Wilmer, M. Leaf, C. Y. Lee, O. K. Farha, B. G. Hauser, J. T. Hupp and R. Q. Snurr, *Nature Chemistry*, 2012, **4**, 83-89.
31. Q. Min Wang, D. Shen, M. Bülow, M. Ling Lau, S. Deng, F. R. Fitch, N. O. Lemcoff and J. Semanscin, *Microporous and Mesoporous Materials*, 2002, **55**, 217-230.
32. P. B. S. Rallapalli, M. C. Raj, S. Senthilkumar, R. S. Somani and H. C. Bajaj, *Environmental Progress & Sustainable Energy*, 2016, **35**, 461-468.
33. G. Li, K. Zhang and T. Tsuru, *ACS Applied Materials & Interfaces*, 2017, **9**, 8433-8436.
34. B. J. Smith and W. R. Dichtel, *Journal of the American Chemical Society*, 2014, **136**, 8783-8789.
35. D. Beaudoin, T. Maris and J. D. Wuest, *Nature Chemistry*, 2013, **5**, 830.
36. T. Ma, E. A. Kapustin, S. X. Yin, L. Liang, Z. Zhou, J. Niu, L.-H. Li, Y. Wang, J. Su, J. Li, X. Wang, W. D. Wang, W. Wang, J. Sun and O. M. Yaghi, *Science*, 2018, **361**, 48.
37. V. Nguyen and M. Grünwald, *Journal of the American Chemical Society*, 2018, **140**, 3306-3311.